Journal of Solid State Chemistry 184 (2011) 463–469

Contents lists available at ScienceDirect

Journal of Solid State Chemistry

journal homepage: www.elsevier.com/locate/jssc

Structural and magnetic properties of $RMn_{2-x}Fe_xD_6$ compounds (R=Y, Er; $x \leq 0.2$) synthesized under high deuterium pressure

V. Paul-Boncour [a,*], S.M. Filipek [b], R. Sato [b], R. Wierzbicki [b], G. André [c], F. Porcher [c], M. Reissner [d], G. Wiesinger [d]

[a] Institut de Chimie et des Matériaux de Paris Est, CMTR, CNRS and U-PEC, 2-8 rue H. Dunant, 94320 Thiais, France
[b] Institute of Physical Chemistry, PAN, UL. Kasprzaka 44/52, 01224 Warsaw, Poland
[c] Laboratoire Léon Brillouin, CEA-CNRS, CEA/Saclay, 91191 Gif-sur-Yvette, France
[d] Institute für Solid State Physics, TU Vienna, Wiedner Haupstrasse 8-10, A1040 Vienna, Austria

ARTICLE INFO

Article history:
Received 7 July 2010
Received in revised form
10 December 2010
Accepted 19 December 2010
Available online 28 December 2010

Keywords:
Laves phase
Deuteride
High pressure
Magnetism
Neutron diffraction

ABSTRACT

$RMn_{2-x}Fe_xD_6$ compounds were obtained by applying a deuterium pressure of several kbar to $RMn_{2-x}Fe_x$ compounds for $x \leq 0.2$ and R=Y, Er. These compounds are isostructural to RMn_2D_6 compounds and crystallize in a K_2PtCl_6 type structure with a random substitution of R and half the Mn atoms in the same 8c site whereas the other Mn atoms are located on the 4a site and surrounded by six D atoms (24e site). According to neutron powder diffraction analysis the Fe atoms are preferentially substituted on the 4a site. $YMn_{2-x}Fe_xD_6$ compounds are paramagnetic and their molar susceptibility follows a modified Curie–Weiss law. $ErMn_{2-x}Fe_xD_6$ compounds display a ferromagnetic behavior at 2 K, but their saturation magnetization ($M_S \sim 4.0$ μ_B/f.u.) is half that of their parent compounds ($M_S \sim 8.0$ μ_B/f.u.). The neutron diffraction patterns of $ErMn_{1.8}Fe_{0.2}D_6$ display below 13 K both ferromagnetic and antiferromagnetic short range order, which can be related to a disordered distribution of Er moments. The paramagnetic temperatures of $ErMn_{2-x}Fe_xD_6$ compounds are negative and decrease versus the Fe content whereas they are positive and increase for their parent compounds.

1. Introduction

Hydrogen absorption in intermetallic compounds has been widely studied for hydrogen storage application but also for the modification of their physical properties [1]. A large amount of studies has been devoted to the magnetic properties of RMn_2H_y and RFe_2H_y Laves phase hydrides, showing a strong interplay between hydrogen and magnetic order depending on the H content [2–5]. For $0 < y \leq 4.5$, hydrogen atoms are located in interstitial sites and form compounds whose structures are derived from the C14 or C15 structure depending on the pristine compounds [3,5–11]. The application of high hydrogen or deuterium pressure (1–12 kbar) on intermetallic compounds resulted in the synthesis of several new metal hydrides/deuterides, with larger H (D) content [12]. This has allowed the synthesis of YFe_2H_5 and $ErFe_2H_5$, which display an orthorhombic distortion derived from the C15 structure [13,14]. More unexpected results have been obtained for RMn_2 compounds (R=Y, Gd, Dy, Ho and Er) which form RMn_2D_6 phases with a new type of cubic structure without relationship with the C15 or C14 structures of the pristine compounds [15–19]. These RMn_2D_6 compounds crystallize in a disordered fluorite structure (K_2PtCl_6 type) which can be described in the *Fm3m* space group where the R and half of the Mn atoms (Mn_1) occupy randomly the 8c site whereas the remaining Mn atoms (Mn_2) are located in the 4a site being surrounded by 6H atoms in the 24e site [16]. This structure is very different from that observed for the other RMn_2H_x hydrides (deuterides) ($0 < x \leq 4.5$) and results from a complete reorganization of the unit cell of the parent compound. YMn_2D_6 is a paramagnet, which follows a modified Curie–Weiss law. The neutron powder diffraction (NPD) study has confirmed the absence of long and short range magnetic order from 1.5 to 290 K in YMn_2D_6. Both $ErMn_2D_6$ and $DyMn_2D_6$ displayed ferro- and antiferromagnetic short range order (SRO) below 10 K, which was attributed to local R–R magnetic interactions. These previous studies have shown that the RMn_2D_6 compounds can be obtained for Y, heavy rare earth elements and even for the whole concentration range in pseudobinary $Y_{1-x}Dy_xMn_2$ compounds [12]. But the influence of the Mn substitution by another transition element on the formation of the RMn_2D_6 phase has not been investigated in detail until now. High pressure hydrogen absorption (7 kbar) applied to ErFeMn led to the formation of $ErFeMnH_{4.7}$, which crystallizes in the same cubic C15 structure as its parent compound with 30% cell volume augmentation [20]. Cubic C15 $YFeMnH_5$ with $\Delta V/V$=29.4% was also obtained under 7 kbar of hydrogen [21].

* Corresponding author. Fax: +33 1 49 78 12 03.
E-mail address: paulbon@icmpe.cnrs.fr (V. Paul-Boncour).

0022-4596/$ - see front matter © 2010 Elsevier Inc. All rights reserved.
doi:10.1016/j.jssc.2010.12.017

The aim of our study was therefore to investigate the possibility to obtain $RMn_{2-x}Fe_xD_6$ compounds for smaller Fe content.

For this purpose $RMn_{2-x}Fe_x$ compounds with R=Y, Er and $x \leq 0.2$ were prepared and submitted to high deuterium pressure. The deuterium thermal desorption was studied by thermogravimetric measurements. Their structural and magnetic properties were studied by X-ray, synchrotron and neutron powder diffraction as well as by magnetic and Mössbauer measurements. These results will be presented and discussed in relation with the structural and magnetic properties of the $RMn_{2-x}Fe_x$ parent compounds and other RMn_2D_6 deuterides.

2. Experimental

$RMn_{2-x}Fe_x$ intermetallic compounds (R=Y and Er, x=0.1 and 0.2) were prepared by induction melting of the pure elements (Y and Er 99.9%: Mn and Fe 99.99%) followed by an annealing treatment of 11 days at 1073 K. The homogeneity of the samples was checked by X-ray diffraction (XRD) and electron probe microanalysis (EPMA).

The synthesis of $RMn_{2-x}Fe_xD_6$ deuterides was carried out at 10 kbar (D_2) and 100 °C. For neutron diffraction about 4 g of $RMn_{1.8}Fe_{0.2}D_6$ samples were prepared in several batches.

Thermal gravimetric analysis (TGA) was performed on a Setsys Evolution 1750 balance from Setaram. The powder was placed in an open Pt crucible and the experiment was performed with an argon flow of 20 ml/min. The temperature was raised at 10 K/min operating from 300 to 1200 K.

The XRD patterns were measured with a D8 Brucker diffractometer equipped with a rear graphite monochromator in the range $10° < 2\theta < 120°$ with a step of 0.02° using Cu $K\alpha$ radiation.

The diffraction patterns of $YMn_{1.8}Fe_{0.2}D_6$ and $ErMn_{1.8}Fe_{0.2}D_6$ were also measured at room temperature using synchrotron radiation (λ=0.501950 Å) provided by SNBL at ESRF in the range $1° < 2\theta < 50°$ with a step of 0.003°.

The NPD patterns of the deuterides were measured at 10 and 300 K on the 3T2 spectrometer and at temperatures varying between 1.4 and 300 K on the G4.1 spectrometer at the Laboratoire Léon Brillouin (LLB) at Saclay. For the experiments on 3T2 the wavelength was 1.225 Å and the angular range $6° < 2\theta < 125°$ with a step of 0.05°. For the experiments on G4.1, the wavelength was 2.427 Å and the angular range was $2° < 2\theta < 82°$ with a step of 0.1°. The deuterides were contained in a vanadium sample holder. All the XRD and NPD patterns were refined with the Rietveld method, using the Fullprof code [22]. The line shapes were refined with a Pearson VII function.

The magnetic measurements were performed with a Physical Properties Measurements System (PPMS) apparatus of Quantum Design operating up to 9 T and from 1.5 to 300 K.

The ^{57}Fe Mössbauer spectrum of $ErMn_{1.8}Fe_{0.2}D_6$ was registered at 294 K during three weeks.

3. Results

3.1. Thermodesorption properties

The $RMn_{2-x}Fe_xD_6$ samples were analyzed by TGA experiments in order to determine the temperature of desorption and the amount of D desorbed. All the samples show a similar thermal desorption behavior, which is displayed as an example for $ErMn_{1.8}Fe_{0.2}D_6$ in Fig. 1. The derivative of the mass variation versus temperature ($\delta m/\delta T$) shows one narrow peak centered at 523 K and a broader one at 612 K. In this range the sample desorbs 3.9(2) D/f.u.. According to the previous results on isostructural RMn_2D_6 compounds this deuterium desorption corresponds to a decomposition into RH_2 and Mn [16–18]. Then at higher temperature an additional desorption process is observed. The derivative curve indicates that the thermodesorption peaks are centered at 1010, 1092 and 1115 K. This further desorption is related to the Er hydride decomposition followed by a recombination with the transition metal to form the starting intermetallic. The desorbed D content is around 0.6 D/f.u., this value is smaller than expected for a complete desorption (2 D/f.u.).

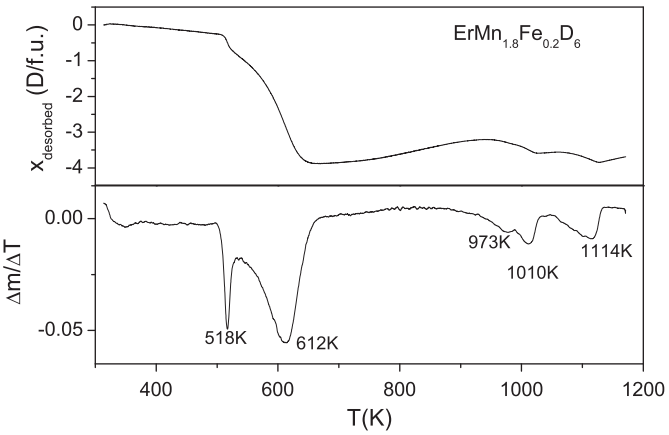

Fig. 1. TGA measurement on $ErMn_{1.8}Fe_{0.2}D_6$: variation of the deuterium content and derivative of the loss of mass.

Table 1
Structure and cell parameters of the $RMn_{2-x}Fe_x$ and $RMn_{2-x}Fe_xD_6$ compounds at 300 K. The data for YMn_2D_6 and $ErMn_2D_6$ are from Refs. [16,17].

Compound	Structure	Space group	a (Å) c (Å)	V (Å^3)	$\Delta V/V$ (%)
YMn_2	C15	$Fd-3m$	7.681(1)	452.98(1)	
YMn_2D_6	Cubic	$Fm3m$	6.709 (1)	301.98(1)	33.3
$YMn_{1.8}Fe_{0.2}$	C15	$Fd-3m$	7.630 (1)	444.20(1)	
$YMn_{1.8}Fe_{0.2}D_6$	Cubic C15	$Fm3m$	6.6970(4)	300.36(1)	35.2
		$Fd-3m$	6.7017(3)[a]	300.99(2)[a]	35.4[a]
			8.253(1)[a]	561.7(1)[a]	26.5[a]
$ErMn_2$	C14	$P63/mmc$	5.2950(1)	209.90(1)	
			8.6446(1)		
$ErMn_2D_6$	Cubic	$Fm3m$	6.6797(1)	298.04(1)	42.0
$ErMn_{1.9}Fe_{0.1}$	C14	$P63/mmc$	5.2888(1)	209.26(1)	
			8.6388(1)		
$ErMn_{1.9}Fe_{0.1}D_6$	Cubic	$Fm3m$	6.6659(6)	296.19(5)	41.5
$ErMn_{1.8}Fe_{0.2}$	C14	$P63/mmc$	5.2783(1)	208.06(1)	
			8.6233(1)		
$ErMn_{1.8}Fe_{0.2}D_6$	Cubic	$Fm3m$	6.6514(5)	294.27(2)	41.4
			6.6690(2)[a]	296.60(1)[a]	42.6[a]

[a] Data from SR measurements.

The desorption peaks appear at the same temperatures for $YMn_{1.8}Fe_{0.2}D_6$ and at slightly lower temperatures for $ErMn_{1.9}Fe_{0.1}D_6$.

3.2. Structural properties

The structure, cell parameters and relative cell volume variation between the $RMn_{2-x}Fe_xD_6$ deuterides and their parent compounds are reported in Table 1. The results of binary RMn_2D_6 compounds from Refs. [16,17] have been added for comparison. YMn_2 and $YMn_{1.8}Fe_{0.2}$ crystallize in the same C15 cubic structure. A decrease of the cell parameter is observed upon Fe substitution in agreement with the smaller atomic radius of Fe compared to Mn. The $ErMn_{2-x}Fe_x$ compounds (x=0, 0.1 and 0.2) crystallize in the hexagonal C14 type structure and their cell parameters also decrease with the Fe content. This is in agreement with the results

of Ref. [23], which showed that the $ErMn_{2-x}Fe_x$ compounds crystallize in the hexagonal C14 phase for $0 \le x \le 0.4$ and in the cubic C15 structure for $x \ge 0.8$.

Deuterium absorption under high gaseous pressure leads to the formation of $RMn_{2-x}Fe_xD_6$ compounds, which crystallize in the same cubic structure as the corresponding RMn_2D_6 compounds. The cubic cell parameter decreases slightly upon Er for Y substitution and upon Fe for Mn substitution. The relative cell volume variation is larger for the Er compounds than for the Y, indicating that the deuterides are less sensitive to the lanthanide contraction than their parent compounds.

The analysis of the synchrotron radiation (SR) patterns shows that $ErMn_{1.8}Fe_{0.2}D_6$ (Fig. 2) is single phase whereas $YMn_{1.8}Fe_{0.2}D_6$ contains 5.3 wt% of a C15 cubic phase with $a=8.2538$ Å. The SR patterns do not show superstructure lines confirming that the Mn and *R* distribution remains random on the 8c site. For both compounds the line widths are very broad compared to the Si reference or even to the intermetallic compounds measured with a classical diffractometer. This broadening is mainly related to isotropic microstrains introduced by the random distribution of *R* and Mn atoms on the same 8c site and was already observed for YMn_2D_6 and $ErMn_2D_6$ [17,24]. The patterns refinement with the Pearson VII function leads to a strain $\delta d/d=2.54\%$ for $ErMn_{1.8}Fe_{0.2}D_6$ and $\delta d/d=2.76\%$ for $YMn_{1.8}Fe_{0.2}D_6$.

NPD experiments were performed on $YMn_{1.8}Fe_{0.2}D_6$ (300 K) and on $ErMn_{1.8}Fe_{0.2}D_6$ (10 and 300 K) in order to determine the localization of the Fe atoms. The difference of neutron coherent scattering length between Fe ($b_c=9.45$ fm) and Mn ($b_c=-3.73$ fm) is large enough to determine the position and occupancy factors of Fe atoms, which is not the case for XRD. The NPD patterns of the $RMn_{1.8}Fe_{0.2}D_6$ compounds were refined like the RMn_2D_6 compounds in the *Fm3m* space group, with a random distribution of *R* and half the Mn atoms on the 8c site; the second half of Mn atoms in the 4a site and the D atoms in the 24e site. Therefore, the Fe atoms can be located either in the 8c site, in the 4a site or in a random mixture of both. The three NPD patterns were refined allowing Fe substitution on both sites, and the refinement converged with a majority of Fe atoms on the 4a site (Table 2). The refined NPD patterns of $ErMn_{1.8}Fe_{0.2}D_6$ at 300 K are plotted in Fig. 3. For $YMn_{1.8}Fe_{0.2}D_6$ only 1.8 wt% of a C15 phase with $a=8.279$ Å was found in the NPD pattern beside the main RMn_2D_6 phase. This percentage of cubic phase is lower than observed in the SR patterns. As the X-rays penetrate only the surface of the sample, whereas the neutrons cross all the sample, this can be an indication that the cubic phase is mainly located at the surface of the grains. The thermal expansion of the cell parameter of $YMn_{1.8}Fe_{0.2}D_6$ is continuous as previously observed for $ErMn_2D_6$ [17] confirming that no structural transition occurs between 1.5 and 300 K. A previous study on YMn_2D_6 has also shown that there is no order–disorder transition above room temperature. As the D atoms are not interstitial but form complex MnH_6 units, they cannot induce a long range order as for $YMn_2H_{4.3}$, which is rhombohedral below 386 K and cubic above this temperature [16].

3.3. Magnetic properties

The thermomagnetization curves ($M(T)$) of $YMn_{1.8}Fe_{0.2}$ and $YMn_{1.8}Fe_{0.2}D_6$ are reported in Fig. 4. The intermetallic compound displays a transition at 205 K, and below a continuous increase of the magnetization down to 2 K. As YMn_2 is antiferromagnetic with T_N around 100 K, this indicates a modification of the magnetic order upon Fe substitution. For the same applied field the magnetization is about 10 times larger for the deuteride compared to the pristine compound. The magnetization curves versus field ($M(H)$) at different temperatures are displayed in Fig. 5. In agreement with the $M(T)$ curves, the $M(H)$ curves of the deuteride are about 10 times larger than for the intermetallic. At 2 K, the $M(H)$ curve displays a weak ferromagnetic behavior but without saturation. Above 50 K, the curves are linear and the dM/dH curves were used to determine the molar susceptibility $\chi_M(T)$ curve of $YMn_{1.8}Fe_{0.2}D_6$, which was

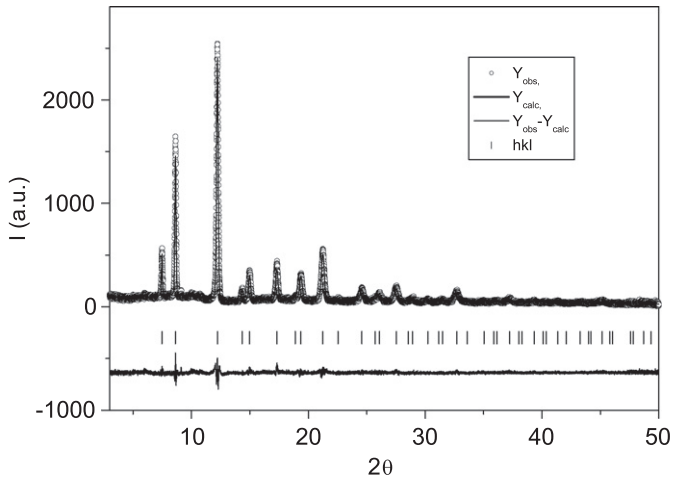

Fig. 2. Refined SR pattern of $ErMn_{1.8}Fe_{0.2}D_6$ at room temperature.

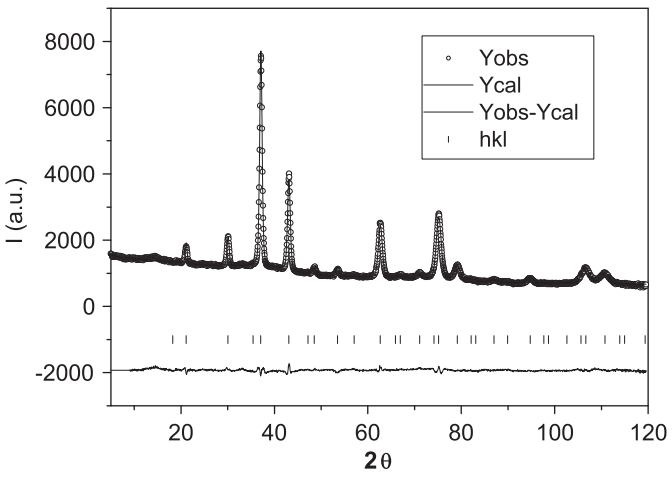

Fig. 3. Refined NPD pattern of $ErMn_{1.8}Fe_{0.2}D_6$ at room temperature.

Table 2
Results of the refinement of the NPD patterns measured on 3T2. In the refinements the total occupancy factor of Fe atoms in the 8c and 4a sites was kept constant and equal to 0.2. The occupancy factors of Fe and Mn atoms were fixed to 1 for each site. The *R*, Mn1 and Fe1 atoms are on the 8c site (¼, ¼, ¼), the Mn_2 and Fe_2 atoms on the 4a site (0, 0, 0) and the D atoms on the 24e site (x_D, 0, 0).

Compound	T (K)	a (Å)	Occ Fe, 8c site	Occ Fe, 4a site	x_D	R_B (%)	R_{wp} (%)
$YMn_{1.8}Fe_{0.2}D_6$	300	6.6987(3)	0.015(2)	0.185(2)	0.2485(3)	6.0	10.2
$ErMn_{1.8}Fe_{0.2}D_6$	10	6.6298(2)	0.009(2)	0.191(2)	0.2479(5)	4.6	9.1
$ErMn_{1.8}Fe_{0.2}D_6$	300	6.6531(3)	0.011(2)	0.189(2)	0.2485(7)	5.5	9.5

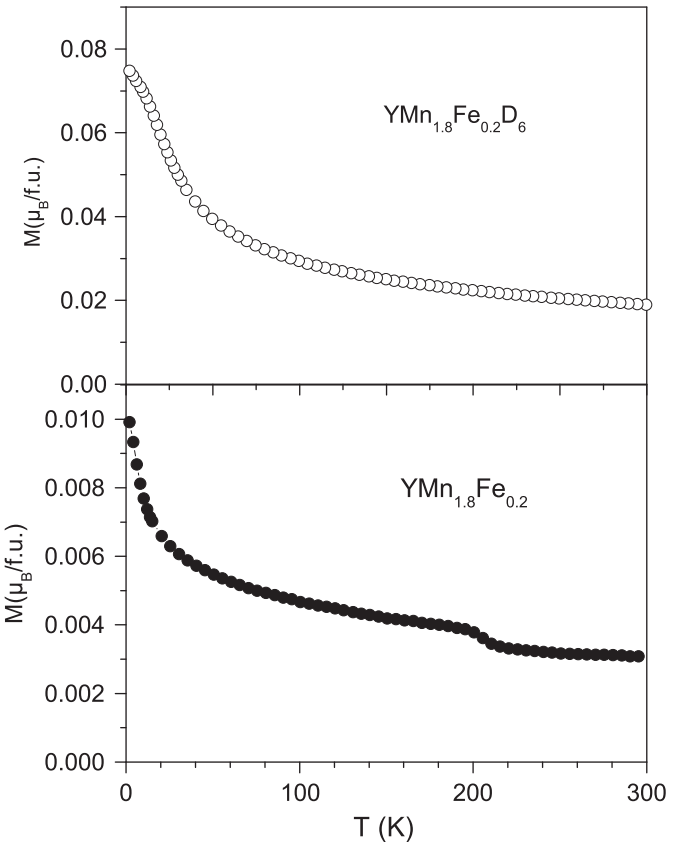

Fig. 4. Thermomagnetization curves of $YMn_{1.8}Fe_{0.2}$ and $YMn_{1.8}Fe_{0.2}D_6$ under an applied field of 15 kOe.

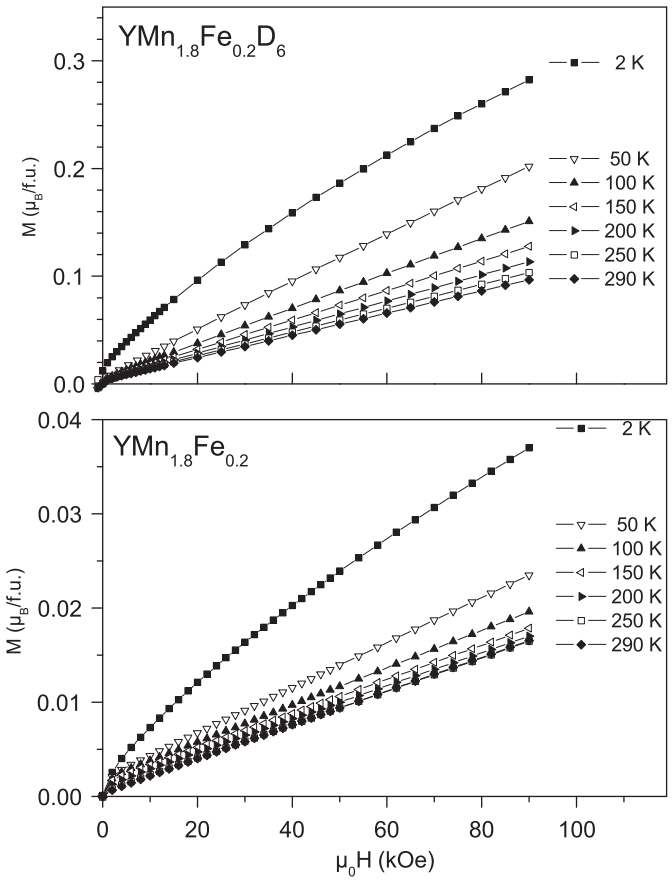

Fig. 5. Magnetization curves at different temperatures of $YMn_{1.8}Fe_{0.2}$ and $YMn_{1.8}Fe_{0.2}D_6$.

fitted with a modified Curie–Weiss (CW) law, as previously done for YMn_2D_6 [16]:

$$\chi_M = \chi_0 + \frac{C}{T-\theta_p} \quad (1)$$

The fit of χ_M leads to $\chi_0 = 0.0046$ emu/mole; $C = 0.825$ emu/mole, $\mu_{eff} = 2.57\ \mu_B$ and $\theta_p = -29$ K, i.e. to a small increase of χ_0 (+0.0006 emu/mole) and μ_{eff} (+0.57 μ_B) compared to YMn_2D_6 values.

The $M(T)$ curves of the $ErMn_{2-x}Fe_x$ compounds and their deuterides are presented in Fig. 6 with an applied field of 300 Oe. The intermetallic compounds show a ferromagnetic behavior with a magnetic ordering temperature of $T_C = 27$ and 34 K for $x = 0.1$ and 0.2, respectively. Compared to C14 $ErMn_2$, a small increase of T_C is observed upon Fe for Mn substitution (Table 3). Magnetic studies on a $ErMn_2$ single crystal have shown a ferromagnetic ordering of the Er moment at 23 K, a spin-canted magnetic structure and a spin reorientation at 10 K [24]. In this compound the Mn atoms have no ordered magnetic moment but display spin fluctuations. As the Fe atoms are substituted in small amount to Mn atoms, they are probably too diluted to induce an ordered magnetic Fe sublattice. The shape of the thermomagnetization curves of the $ErMn_{2-x}Fe_x$ samples with $0 \le x \le 0.2$ are very similar and only shifted to higher temperature.The increase of T_C is therefore rather related to the shortening of Er–Er distances according to the RKKY model.

No clear ferromagnetic transition temperature is observed in the deuterides. The $M(H)$ curves of these compounds, presented in Fig. 7 for $ErMn_{1.8}Fe_{0.2}$ and its deuteride, were refined in order to determine the saturation magnetization and the molar susceptibility. At 2 K, the saturation magnetization extrapolated at zero field (M_S) of the intermetallic compounds are around 8.1(1) μ_B/f.u. close to the 8.3 μ_B/f.u. measured in $ErMn_2$ at 4.2 K and 140 kOe [24]. This confirms that the contribution of Fe to the saturation magnetization is weak or negligible. The magnetization of the deuterides extrapolated to zero field is only 4.0(2) μ_B/f.u. In addition, at 9 T the saturation is still not reached for the deuterides. The lowering of the magnetization and the absence of saturation can be explained by a strong canting of Er moments or by a coexistence of ferromagnetic and antiferromagnetic domains in the deuterides. The paramagnetic values reported in Table 3, show an increase of θ_p and a slight decrease of μ_{eff}/f.u. as the Fe content increases in the intermetallic compounds. Concerning the deuterides, μ_{eff} is not very sensitive to the Fe content; θ_p is negative and decreases slightly with the Fe content. The change of sign of θ_p between the intermetallic and the deuterides indicates, in agreement with the variation of M_S, that the magnetic order changes from ferromagnetic to ferri or antiferromagnetic order upon deuteriation. In order to elucidate the type of magnetic order in the deuterides, NPD measurements were necessary.

The comparison of the NPD patterns of the $YMn_{1.8}Fe_{0.2}D_6$ measured on G4.1 at different temperatures shows mainly a line displacement due to thermal expansion. For $ErMn_{1.8}Fe_{0.2}D_6$, besides the peak displacement, a change of background intensity is observed at low angle and below 30 K (Fig. 8). The difference patterns between $T_1 = 1.4$–13 K and $T = 30$ K are presented in the inset of Fig. 8. At angles lower than $2\theta = 15^\circ$, the decrease of background intensity versus the angle can be attributed to ferromagnetic SRO [25] and its intensity decreases as T_1 increases. As this background variation at low angle was not observed for $YMn_{1.8}Fe_{0.2}D_6$ it should be related to the magnetic contribution of Er moment.. A broad line centered around $2\theta = 30^\circ$ or $d = 4.747$ Å is also observed in the difference curves. This value is slightly larger

than the average distance $d=4.703$ Å between two Er next neighbors in the 8c site. As this bump is observed also at room temperature, but with a lower intensity, it should correspond to both nuclear and magnetic SRO. The nuclear contribution should be related to the chemical disorder (Mn, Er) observed on the 8c site. The magnetic intensity of this broad line decreases only slightly with T_1 and can be related to AF interactions as it was already observed in $ErMn_2D_6$ [17].

A ^{57}Fe Mössbauer spectrum has been measured for $ErMn_{1.8}Fe_{0.2}D_6$ at 294 K. Due to the small Fe content compared to $ErFe_2D_5$ (Fig. 9) intensity and statistics of the spectrum are rather poor. The spectrum was fitted with a broad doublet ($\Gamma=0.33\pm0.01$ mm/s), only slightly broader than that obtained for $ErFe_2D_5$, showing a much better statistics ($\Gamma=0.31\pm0.01$), with an isomer shift (IS) of -0.09 ± 0.01 mm/s relative to alpha iron and a quadrupole splitting (QS) of 0.30 ± 0.01 mm/s. In [23], the authors have investigated the structural and magnetic properties of $ErMn_{2-x}Fe_x$ compounds. No significant change of the isomer shift upon the Mn content was obtained. For the Mn rich compound $ErMn_{1.6}Fe_{0.4}$, crystallizing in the C14 structure, the QS was found to be around 0.22 mm/s, i.e. two-thirds of QS=0.33 mm/s which was obtained for $ErMn_{0.8}Fe_{1.2}$. An even a smaller QS should be observed

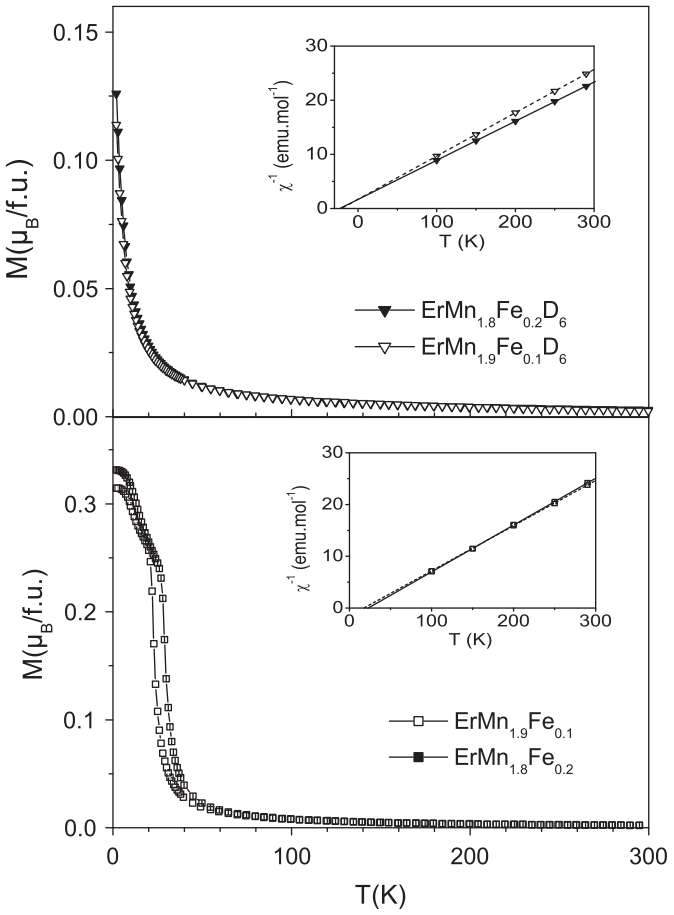

Fig. 6. Thermomagnetization curves of $ErMn_{2-x}Fe_x$ and $ErMn_{2-x}Fe_xD_6$ at 300 Oe. *Inset*: the symbols correspond to the H/M values deduced from the $M(H)$ curves and the line to the linear fit.

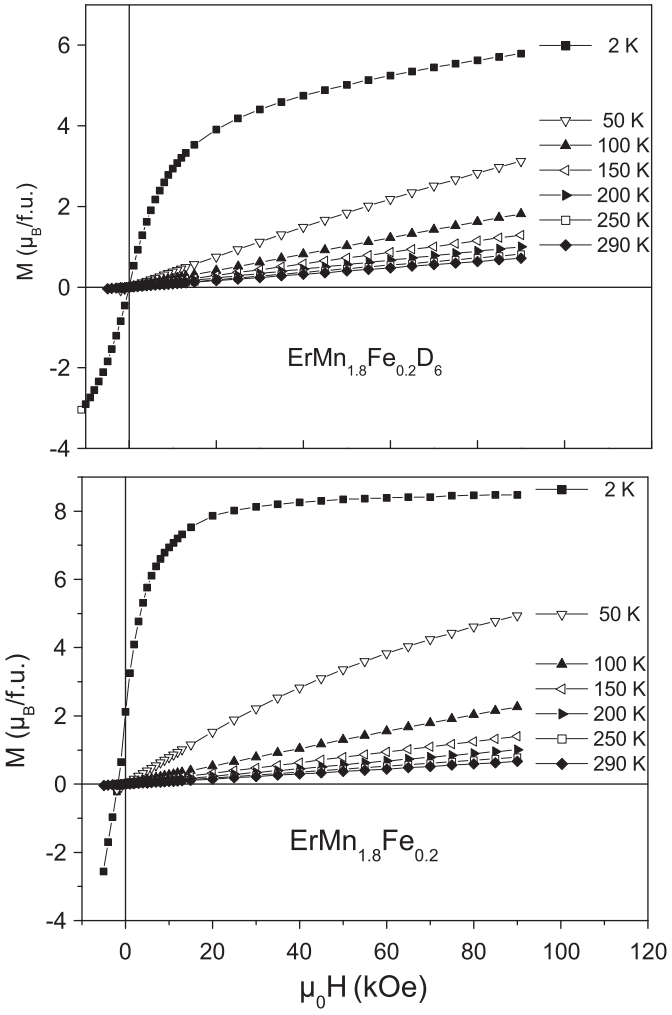

Fig. 7. Magnetization curves of $ErMn_{1.8}Fe_{0.2}$ and $ErMn_{1.8}Fe_{0.2}D_6$.

Table 3
Magnetic properties of $RMn_{2-x}Fe_x$ and $RMn_{2-x}Fe_xD_6$ ($x=0$, 0.1 and 0.2) compounds.

Compound	M_S (2 K) (μ_B/f.u.)	T_N (K)	T_C (K)	θ_p (K)	C (emu/mol.Oe)	μ_{eff} (μ_B/f.u.)
YMn_2		100.0(1)				
YMn_2D_6	0.53[a]			−30.0(2)	0.55(1)	3.0(1)[b]
$YMn_{1.8}Fe_{0.2}$	0.007(1)		210.0(1)			
$YMn_{1.8}Fe_{0.2}D_6$	0.074(1)			−29.0(2)	0.83(1)	2.6(1)[b]
$ErMn_2$	8.1(1)		25.0(2)	8.0(1)	12.61(1)	10.0(1)
$ErMn_2D_6$	5.0(1)		–	−15.4(1)	13.58(1)	10.4(1)
$ErMn_{1.9}Fe_{0.1}$	8.1(1)		27.0(2)	18.1(2)	11.45(1)	9.6(1)
$ErMn_{1.9}Fe_{0.1}D_6$	3.8(1)		–	−21.3(3)	12.70(1)	10.1(1)
$ErMn_{1.8}Fe_{0.2}$	8.2(1)		34.4(2)	22.6(2)	11.18(1)	9.5 (1)
$ErMn_{1.8}Fe_{0.2}D_6$	4.1(1)		–	−23.3(3)	14.11(2)	10.6(1)

[a] Measured at 5 K.
[b] The μ_{eff} are by Mn atom. The data for YMn_2D_6 and $ErMn_2D_6$ are from Refs. [16,17].

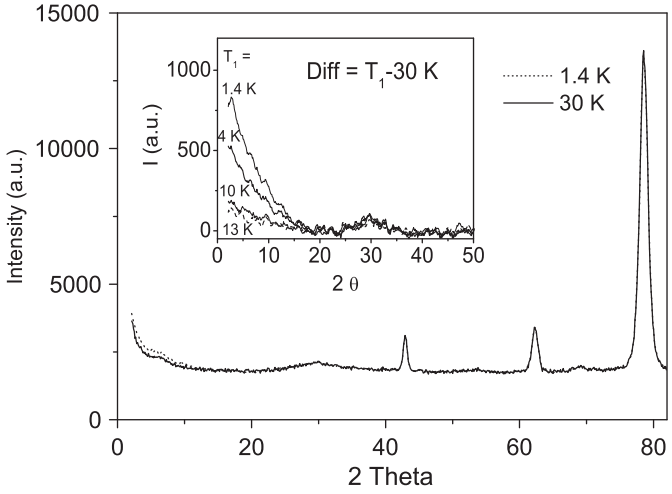

Fig. 8. NPD patterns of $ErMn_{1.8}Fe_{0.2}D_6$ at 1.4 and 30 K measured on G4.1. *Inset*: difference curves between the NPD patterns measured at T_1 and 30 K.

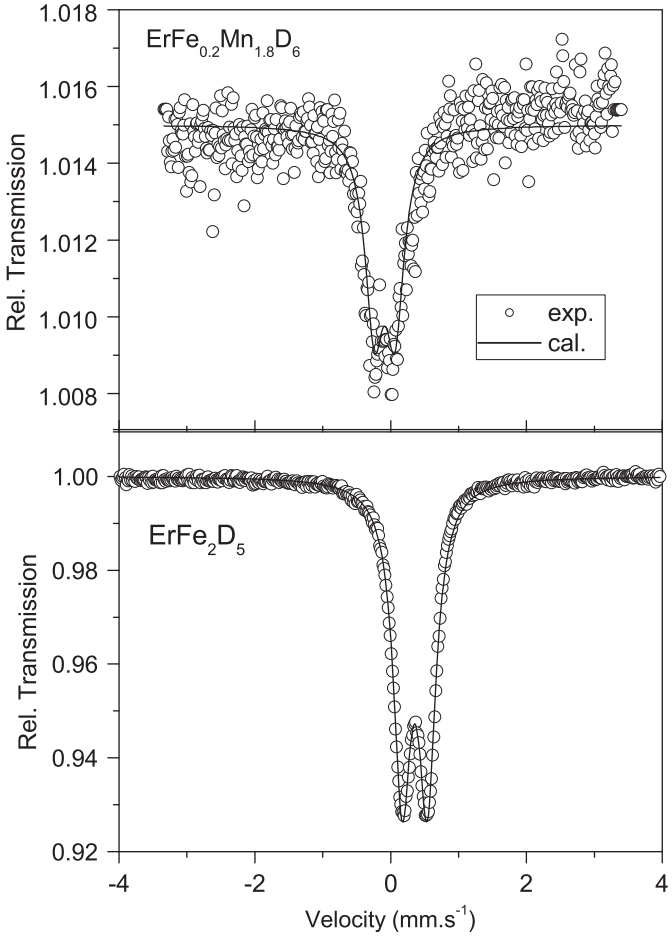

Fig. 9. Mössbauer spectra of $ErFe_{0.2}Mn_{1.8}D_6$ compared to that of $ErFe_2D_5$ at 294 K.

for $ErMn_{1.8}Fe_{0.2}$, say around QS = 0.2 mm/s. Thus, we have to face a large deuterium induced increase in quadrupole splitting of about 0.1 mm/s, i.e. 50%. On the other hand, surprisingly, we obtain still a negative isomer shift (IS = −0.09 mm/s) for the deuteride, only somewhat more positive than that which would be expected [22] for the parent compound, (IS ≈ −0.26 mm/s). Since a substantial volume increase is accompanied by deuterium uptake, this points to some rise of the s-electron density at the Fe nucleus upon deuteration. Commonly, however, a substantial increase of IS towards positive values is observed upon hydrogen or deuterium absorption in interstitial sites, which was attributed to a decrease in s-electron density at the Mössbauer nucleus [14,26–28]. As in $ErMn_{1.8}Fe_{0.2}D_6$ the Fe atoms are surrounded by six D atoms with a strong Fe–H bond, this can explain the small negative value of IS compared to the positive one of interstitial hydrides and deuterides. It is closer to the IS of Mg_2FeD_6 which is 0.02 mm/s with respect to α-Fe at room temperature [29].

4. Discussion

This study has shown that for $x \leq 0.2$, $RMn_{2-x}Fe_xD_6$ phases with a disordered K_2PtCl_6 structure can be obtained after applying 10 kbar deuterium pressure at 100 °C. A previous study has shown that this phase could not be obtained for a larger Fe content: even under several kbar of hydrogen ErMnFe form an hydride with a cubic C15 type structure and 4.7 H/f.u. [20]. A current work on YFeMn also shows that the hydrides synthesized under high hydrogen pressure crystallize in a C15 cubic structure with 5 H/f.u [21]. The largest value of substituted Fe which still allow to obtain the K_2PtCl_6 phase has to be determined more precisely in the range $0.2 < x < 1$, but the presence of a C15 deuteride contribution in $YMn_{1.8}Fe_{0.2}D_6$ suggests that we are very close to this limit.

The study of deuterium absorption in $YMn_{2-x}Fe_x$ compounds for deuterium pressures below 1 bar has shown that the $YMn_{2-x}Fe_xD_{4.3}$ phase crystallizes in the same rhombohedral structure as $YMn_2D_{4.3}$ for $0 \leq x \leq 0.2$, in a cubic C15 structure with a disordered deuterium sublattice for $0.2 < x < 1.7$, and in a $YFe_2D_{4.2}$ monoclinic structure for $x \geq 1.7$ [25]. Further investigations will be undertaken to establish more precisely the limit of existence of the $RMn_{2-x}Fe_x$ hydrides or deuterides synthesized under high hydrogen pressure. But it is expected that the compound isostructural to cubic YMn_2H_6 or to orthorhombic YFe_2H_5 exists only in a limited range of concentration in the Mn and Fe rich side, respectively.

The NPD results showed that for both $YMn_{1.8}Fe_{0.2}D_6$ and $ErMn_{1.8}Fe_{0.2}D_6$, the Fe atoms are preferentially substituted on the 4a site, i.e. on the site surrounded by six D atoms. The origin of this preferential occupation can be either geometric or electronic. From the geometric point of view, Fe has a smaller atomic radius (r_{Fe} = 1.25 Å) than Mn (r_{Mn} = 1.35 Å). On the 8c site the Mn atoms occupy the same site as Y or Er atoms. The difference of radius between R and Mn atoms is already large (r_Y = 1.801 Å, r_{Er} = 1.757 Å). Therefore, substituting a smaller atom on this site may introduce too much additional stresses. On the 4a site, the geometric constrains are smaller, as Fe atoms replace only Mn atoms. The variation of the cell parameters versus the rate of substituted Fe atoms indicates that the structure is sensitive to the atomic size difference between Mn and Fe atoms. The $RMn_{2-x}Fe_xD_6$ compounds are isostructural to complex metal hydrides M_2TH_6 where M is a divalent alkaline earth (M = Mg, Ca, Sr) or a divalent rare earth metal (M = Eu, Yb) and M' a transition metal (M' = Fe, Ru, Os) [30,31]. It was therefore previously suggested that the RMn_2D_6 compounds have the $(R^{III}Mn^{I})^{4+}(Mn^{II}D_6)^{4-}$ configuration according to the 18^{e-} rules [16]. In isostructural Mg_2FeH_6, the Fe atoms are located on the 4a site forming octahedral FeH_6^{4-} anions and experimental results were in favor of a low-spin Fe^{II} configuration [29]. Therefore both geometric and electronic factors can favor the localization of Fe on the 4a site.

The $M(T)$ curves of $YMn_{1.8}Fe_{0.2}$ indicate a weak transition at 205 K, however according to Hilscher et al. [32], T_C = 200 K is obtained for $YMn_{0.2}Fe_{1.8}$, and a ferromagnetic order is observed only for $x > 0.6$. Therefore this transition may originate from a small amount of second phase with a larger amount of Fe and not

observed by XRD. For $ErMn_{2-x}Fe_x$ compounds, a small increase of T_C from 25 to 33.7 K is observed as x increases from 0 to 0.2. This change of T_C is small compared to T_C=220 K measured for ErFeMn [20]. Previous studies [23] on $ErMn_{2-x}Fe_x$ compounds showed also a decrease of T_C upon Fe for Mn substitution from 580 K (x=2) to about 440 K (x=1.6). Mössbauer spectra at 300 K, displayed only a doublet for $x<1.2$ indicating that T_C is reduced below room temperature for larger Mn content. It can be assumed that like for $YMn_{2-x}Fe_x$ compounds [32,33], there is a critical Fe concentration necessary to observe a ferromagnetic behavior on the Fe sublattice, and that the change of T_C for low Fe content is mainly related to the Er magnetic order. The smaller cell volume should induce a decrease of the average Er–Er distances and consequently an increase of the Er–Er interactions which can influence the magnetic ordering temperature.

The magnetic susceptibility of $YMn_{1.8}Fe_{0.2}D_6$ has a behavior close to that of YMn_2D_6, following a modified Curie–Weiss behavior. The fit of χ_M leads to a small increase of μ_{eff} from 2 to 2.6 μ_B due to the Fe for Mn substitution.

The saturation magnetizations of $ErMn_{2-x}Fe_xD_6$ are about half those of the parent compounds. This can be explained by the coexistence of SRO ferromagnetic and antiferromagnetic contributions observed by NPD. The values of μ_{eff} increase slightly between x=0 and x=0.2 reaching 10.6 μ_B. The difference of 0.4 μ_B is slightly smaller than that observed for the Y compounds. The main influence of the Fe substitution is a shift of θ_p to more negative values, which means a stabilization of the AF interactions. As the NPD data showed that the AF contribution is maintained to a larger temperature T_1, than the ferromagnetic one, this means that the Fe substitution stabilizes the antiferromagnetic interactions between Er moments. As discussed before this can be a consequence of a change of Er–Er distances due to the decrease of the cell parameter since the Er–Er interactions follow a RKKY model which is very sensitive to the change of inter-atomic distances.

In order to determine the evolution of the structural and magnetic properties for larger Fe content further experiments will be performed.

5. Conclusions

Deuterides isostructural to the RMn_2D_6 phases (R=Y, Er) were successfully synthesized by submitting $RMn_{2-x}Fe_x$ compounds with $x \leq 0.2$–10 kb deuterium pressure. The Fe for Mn substitution leads to a decrease of the cell parameter, which is relatively more important for the Er compounds. The NPD analysis shows that Fe atoms are mainly substituted on the 4a site. The magnetic properties are slightly modified upon Fe substitution. The $YMn_{2-x}Fe_xD_6$ compounds follow a modified Curie–Weiss behavior with a small increase of μ_{eff} with Fe content. The $ErMn_{2-x}Fe_xD_6$ compounds present a coexistence of ferromagnetic and antiferromagnetic SRO at low temperature, which is explained by the random distribution of the Er moments on the 8c site. The AF contribution is stabilized by the Fe substitution as θ_p becomes more negative and the SRO AF contribution is more stable than the ferromagnetic one as the temperature increases.

Acknowledgments

We are thankful to E. Leroy for the EPMA analysis. We thank Mr Latroche for the synchrotron measurements at ESRF. Support from Grant of MNiSW No. N N204 527939 is gratefully acknowledged. The neutron experiments at LLB have been also supported by NMI3 Project no. 8696. We are thankful to Mrs. F. Bourée for her support to this NMI3 project.

References

[1] G. Wiesinger, G. Hilscher, in: K.H.J. Buschow (Ed.), Handbook of Magnetic Materials, vol. 17, Elsevier, North-Holland, Amsterdam, 2008, p. 293.
[2] V. Paul-Boncour, J. Alloys Compd. 367 (2004) 185.
[3] I.N. Goncharenko, I. Mirebeau, A.V. Irodova, E. Suard, Phys. Rev. B 56 (1997) 2580.
[4] I.N. Goncharenko, I. Mirebeau, A.V. Irodova, E. Suard, Phys. Rev. B 59 (1999) 9324.
[5] O.L. Makarova, I.N. Goncharenko, A.V. Irodova, I. Mirebeau, E. Suard, Phys. Rev. B 66 (2002) 104423.
[6] V. Paul-Boncour, L. Guénée, M. Latroche, A. Percheron-Guégan, J. Alloys Compd. 255 (1997) 195.
[7] V. Paul-Boncour, L. Guénée, M. Latroche, A. Percheron-Guégan, B. Ouladdiaf, F. Bourée-Vigneron, J. Sol. State Chem. 142 (1999) 120.
[8] K.H.J. Buschow, R.C. Sherwood, J. Appl. Phys. 48 (1977) 4643.
[9] H. Fujii, M. Saga, T. Okamoto, J. Less, Common Met. 130 (1987) 25.
[10] J. Przewoznik, V. Paul-Boncour, M. Latroche, A. Percheron-Guégan, J. Alloys Compd. 225 (1995) 436.
[11] J. Przewoznik, V. Paul-Boncour, M. Latroche, A. Percheron-Guégan, J. Alloys Compd. 232 (1996) 107.
[12] S.M. Filipek, V. Paul-Boncour, N. Kuriyama, N. Takeichi, H. Tanaka, R.-S. Liu, R. Wierzbicki, R. Sato, H.-T. Kuo, Solid State Ionics 181 (2010) 306.
[13] V. Paul-Boncour, S.M. Filipek, A. Percheron-Guégan, I. Marchuk, J. Pielaszek, J. Alloys Compd. 317-318 (2001) 83.
[14] V. Paul-Boncour, S.M. Filipek, I. Marchuk, G. André, F. Bourée, G. Wiesinger, A. Percheron-Guégan, J. Phys.: Condens. Matter 15 (2003) 4349.
[15] C.-Y. Wang, V. Paul-Boncour, R.-S. Liu, A. Percheron-Guégan, M. Dorogova, I. Marchuk, T. Hirata, S.M. Filipek, H.-S. Sheu, L.-Y. Jang, J.-M. Chen, H.-D. Yang, Solid State Commun. 130 (2004) 815.
[16] V. Paul-Boncour, S.M. Filipek, M. Dorogova, F. Bourée, G. André, I. Marchuck, A. Percheron-Guégan, R.S. Liu, J. Sol. State Chem. 178 (2005) 356.
[17] V. Paul-Boncour, S.M. Filipek, G. André, F. Bourée, M. Guillot, R. Wierzbicki, I. Marchuk, R.S. Liu, B. Villeroy, A. Percheron-Guégan, H.-D. Yang, S.C. Pin, J. Phys.: Condens. Matter 18 (2006) 6409.
[18] V. Paul-Boncour, S.M. Filipek, R. Wierzbicki, G. André, F. Bourée, M. Guillot, J. Phys.: Condens. Matter 21 (2009) 016001.
[19] S.M. Filipek, H. Sugiura, V. Paul-Boncour, R. Wierzbicki, R.S. Liu, N. Bagkar, J. Phys.: Conf. Ser. 121 (2008) 022001.
[20] S. Mylswamy, V. Drozd, R.S. Liu, N.C. Bagkar, C.C. Chou, C.P. Sun, H.D. Yang, V. Paul-Boncour, I. Marchuk, S.M. Filipek, H.-S. Sheu, L.-Y. Jang, New J. Phys. 9 (2007) 271.
[21] V. Drozd, H.T. Kuo, N. Bagkar, S. Mylswamy, R.S. Liu, V. Paul-Boncour, I. Marchuk, S.M. Filipek, C.C. Chou, C.P. Sun, H.D. Yang, J.M. Chen, Int. J. Hydrogen Energy, in press, doi:10.1016/j.ijhydene.2010.09.010.
[22] J. Rodríguez-Carvajal, in: Proceedings of the Congress of the International Union of Crystallography, 1990, p. 127.
[23] A.S. Ilyushin, W.E. Wallace, J. Sol. State Chem. 17 (1976) 131.
[24] E. Talik, M. Kulpa, T. Mydlarz, J. Kusz, H. Bohm, J. Alloys Compd. 348 (2003) 12.
[25] P. Cadavez-Peres, I.N. Goncharenko, I. Mirebeau, Appl. Phys. A 74 (2002) S692.
[26] V. Paul-Boncour, G. Wiesinger, C. Reichl, M. Latroche, A. Percheron-Guégan, R. Cortes, Phys. B: Condens. Matter 307 (2001) 277.
[27] V. Paul-Boncour, C. Giorgetti, G. Wiesinger, A. Percheron-Guégan, J. Alloys Compd. 356-357 (2003) 195.
[28] T. Okamoto, H. Fujii, S. Takeda, T. Hirara, J. Less, Common Met. 88 (1982) 181.
[29] J.-J. Didisheim, P. Zolliker, K. Yvon, P. Fischer, J. Schefer, M. Gubelmann, A.F. Williams, Inorg. Chem. 23 (1984) 1953.
[30] E. Orgaz, M. Gupta, J. Phys.: Condens. Matter 5 (1993) 6697.
[31] H. Kohlmann, third edition, Encyclopedia of Physical Science and Technology, vol. 9, Academic Press, 2002, p. 441.
[32] G. Hilscher, H.R. Kirchmayr, J. Phys. 5 (1979) 196.
[33] J.-W. Cai, Y.-B. Feng, H.L. Luo, Z. Zeng, Q.-Q. Zheng, J. Appl. Phys. 76 (1994) 7043.